Available online at www.sciencedirect.com

SciVerse ScienceDirect

Ceramics International 39 (2013) 8173–8181

CERAMICS INTERNATIONAL

www.elsevier.com/locate/ceramint

Microstructures and ablation properties of C/C–SiC–ZrC composites prepared using C/C skeletons with various densities

Zhaoqian Li[a,b], Hejun Li[a,*], Shouyang Zhang[a], Wei Li[a], Jie Wang[a]

[a]*State Key Laboratory of Solidification Processing, C/C Composites Research Centre, Northwestern Polytechnical University, Xi'an 710072, PR China*

[b]*Shanghai Aerospace Equipment Manufacture, Shanghai 200245, PR China*

Received 15 November 2012; received in revised form 8 March 2013; accepted 29 March 2013
Available online 8 April 2013

Abstract

Two-dimensional C/C–SiC–ZrC composites were prepared by isothermal chemical vapour infiltration combined with the reaction melt infiltration method using various density porous C/C skeletons. The microstructures, mechanical properties and ablation behaviour of the C/C–SiC–ZrC composites were systematically studied. The results showed that the strength and ablation resistance of C/C–SiC–ZrC composites improved with the increase of the C/C skeleton density. When the density of the C/C skeleton was 1.51 g/cm^3, the bending modulus and strength of the composites were 13.19 GPa and 70.57 MPa, respectively, and the linear and mass ablation rates of the composites ablated for 90 s were 1.44×10^{-3} mm/s and 0.21×10^{-3} g/s, respectively. These properties were attributed to the introduction of ZrC and SiC into the matrix and the formation of a dense SiC–ZrC coating on the surface. The SiC–ZrC coating acted as an oxygen diffusion barrier for C/C composites and first reacted with oxygen to form an oxide protecting layer in the ablation environment.

Keywords: C. Corrosion; C. Strength; C/C–SiC–ZrC composites; Reaction melt infiltration; Microstructures

1. Introduction

There is an increasing demand for advanced materials with a temperature capability of over 2000 °C for ultrahigh temperature and aerospace applications. Carbon/carbon (C/C) composites are considered as one of the most promising candidates for the aerospace applications, such as rocket engines, nose cones and leading edges of re-entry vehicles, because of their low density, high strength-to-weight ratio, good thermal shock resistance and good ablation resistance at elevated temperatures [1–3]. However, the fact that C/C composites oxidize at temperature as low as 700 K has strictly limited their high temperature applications [4–8]. It is necessary to develop protective anti-oxidation and anti-ablation materials to prevent oxidation and the consequential gasification in an ablative environment with high-pressure gas flow and ultrahigh temperatures (> 2000 °C).

One effective solution to improve the ablation resistance of C/C composites is to introduce ultra-high temperature ceramics such as SiC, ZrC, ZrB_2 and HfB_2 into the matrix or coating [9–12]. Some researches show that C/C−SiC composites have excellent anti-oxidation resistance at 1600 °C but cannot meet the requirements because of their rapid ablation at the scouring of the ultrahigh temperatures and high pressure flux [13,14]. Further modification for C/C−SiC composites is necessary. ZrC is an advanced ceramic with a high melting point (3540 °C), excellent chemical stability and resistance to thermal shock [15,16]. In addition, its oxide can effectively reduce the diffusion of oxygen. So far, there are only a few reports about the fabrication and properties of C/C−SiC−ZrC composites. Wang et al. [17] prepared C/C–SiC–ZrC composites by the reactive melt infiltration (RMI) method with molten $Si_{0.87}Zr_{0.13}$ alloy. Wu et al. [18] prepared two-dimensional (2D) C/C−ZrC−SiC composites through precursor infiltration and the pyrolysis (PIP) process using a hybrid precursor containing polycarbosilane and organic zirconium containing polymeric precursor. We have also fabricated integer felt reinforced (1D) C/C–SiC–ZrC composites by isothermal chemical vapour infiltration (ICVI) combined with the RMI method in the previous work [19]. Further investigations on the fabrication, mechanical properties and

*Corresponding author. Tel.: +86 29 88495004; fax: +86 29 88492642.
E-mail address: lihejun@nwpu.edu.cn (H.J Li).

0272-8842/$ - see front matter © 2013 Elsevier Ltd and Techna Group S.r.l. All rights reserved.
http://dx.doi.org/10.1016/j.ceramint.2013.03.093

erosion behaviour of C/C–SiC–ZrC composites are of considerable importance for their application at high temperature.

In this paper, 2D needled felt C/C–SiC–ZrC composites were prepared by ICVI combined with the RMI method using various density porous C/C skeletons. The microstructures, mechanical properties and ablation resistance of the C/C–SiC–ZrC composites were systematically investigated. The experimental results are helpful to improve the theoretical system of the C/C–SiC–ZrC composites.

2. Experimental

2.1. Material preparation

2D carbon felts with a density of 0.47 g/cm^3 which were fabricated by alternatively stacked non-woven layers and carbon fibre webs by a needle-punching technique were used as reinforcement for C/C composites. The volume content of the felt was about 24.5%. Carbon matrix was introduced into the felt by ICVI at 1000−1100 °C using natural gas (CH_4) as precursor to form porous C/C skeletons, followed by a graphitization process at 2500 °C for 2 h. The density of the porous C/C skeletons was controlled to be approximately 1.12, 1.30 and 1.51 g/cm^3 (labelled as CC-1, CC-2 and CC-3, respectively) when deposited for 40, 48 and 80 h, respectively.

The as-prepared C/C skeletons wrapped with Zr, Si, C and ZrO_2 powders according to the mole ratio Zr:Si:C:ZrO_2 of 3:5:1:0.2 were heat-treated in argon protective atmosphere at 2300 °C for 2 h to obtain the C/C−SiC−ZrC composite samples (labelled as CSZ-1, CSZ-2 and CSZ-3, correspondingly). All the above powders, with the granularities of 300 meshes, were of analytical grade and mixed by a blender for 4 h. ZrO_2 and C powders were introduced into the pack chemistry to increase the rate of diffusing reaction and improve the compactness of the coating. The specimens CSZ-1 to CSZ-3 were fabricated using CC-1 to CC-3, respectively.

2.2. Mechanical property testing

The bending strength of the composites was measured using a three-point bending test (SANS CMT 4304, Sans Testing Machine, China) with a span of 40 mm. The load velocity was 0.05 mm/min. At least three samples with a dimension of $55 \times 10 \times 4$ mm^3 were tested to obtain the average data. The stress–strain curves were recorded by computer along with testing.

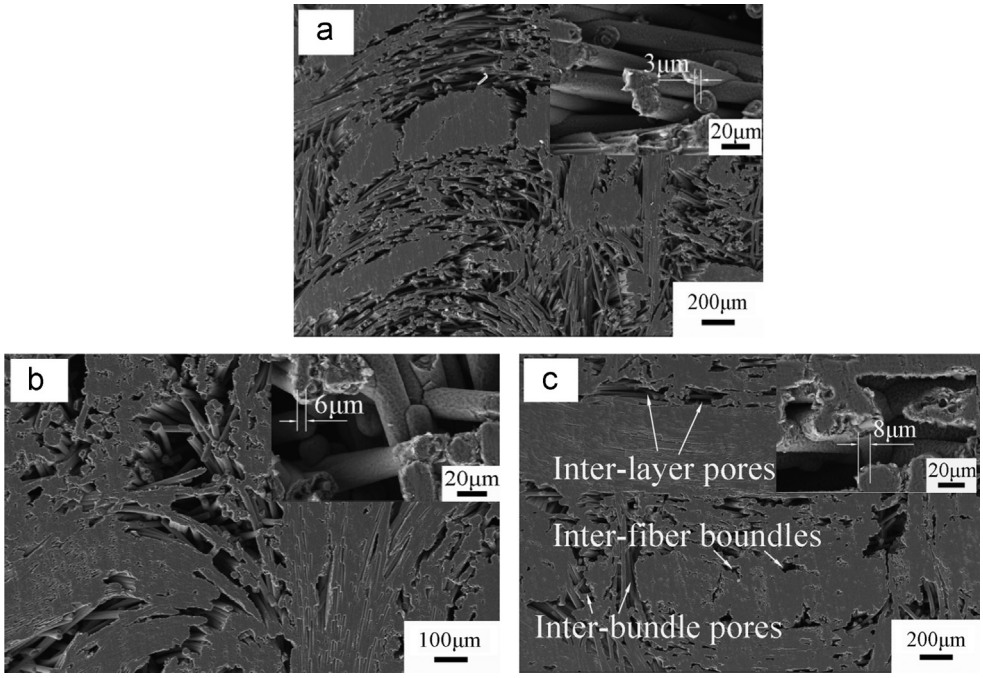

Fig. 1. The SEM graphs of the C/C skeletons prepared to different densities using the ICVI process: (a) CC-1 deposited for 40 h; (b) CC-2 deposited for 48 h and (c) CC-3 deposited for 80 h. The insets display the thickness of PyC covered on fibres.

Table 1
The density, open porosity and closed porosity of the C/C composites and the C/C−SiC−ZrC composites.

Samples	CC-1	CC-2	CC-3	CSZ-1	CSZ-2	CSZ-3
Density (g/cm^3)	1.12 ± 0.02	1.30 ± 0.03	1.51 ± 0.02	1.78 ± 0.05	1.95 ± 0.04	1.86 ± 0.05
Open porosity (%)	45.01 ± 0.15	34.52 ± 0.11	25.16 ± 0.06	6.83 ± 0.08	0.18 ± 0.11	0.30 ± 0.04
Closed porosity (%)	0.57 ± 0.05	0.86 ± 0.06	1.33 ± 0.13	0.53 ± 0.10	0.81 ± 0.06	1.24 ± 0.15

2.3. Ablation testing

The ablation behaviour of 2D C/C–SiC–ZrC composites was tested with an oxyacetylene torch, which was close to the practical ablative situation for aerospace materials. At least three samples with a dimension of Φ30 mm × 10 mm were used in the test. The temperature of the oxyacetylene torch was measured using an optical pyrometer and reached up to 2300 °C. The exposure time under the torch flame was 30 s, 60 s and 90 s. The linear and mass ablation rates of the samples were evaluated by the thickness and mass changes after ablation, respectively. Further details about the test process were described elsewhere [19].

2.4. Characterizations

Phase analysis of 2D C/C–SiC–ZrC composites was carried out by X-ray diffraction (XRD, Philips X'Pert MPD, Holland) using CuKα radiation. The microstructures and morphologies of the samples were analysed using field emission scanning electron microscopy (FESEM, Zeiss-Supra 55) along with Electron Dispersive X-Ray Spectroscopy (EDX, Oxford-INCAPentaFET-3) for chemical analysis. The density, open porosity and closed porosity of the composites were measured by a water penetration technique according to the ASTM C20-00 standard.

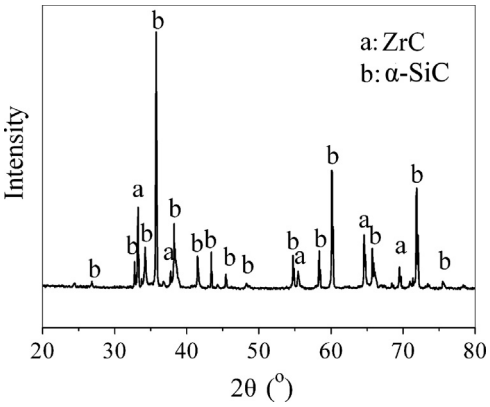

Fig. 3. XRD pattern of the surface of composites CSZ-3.

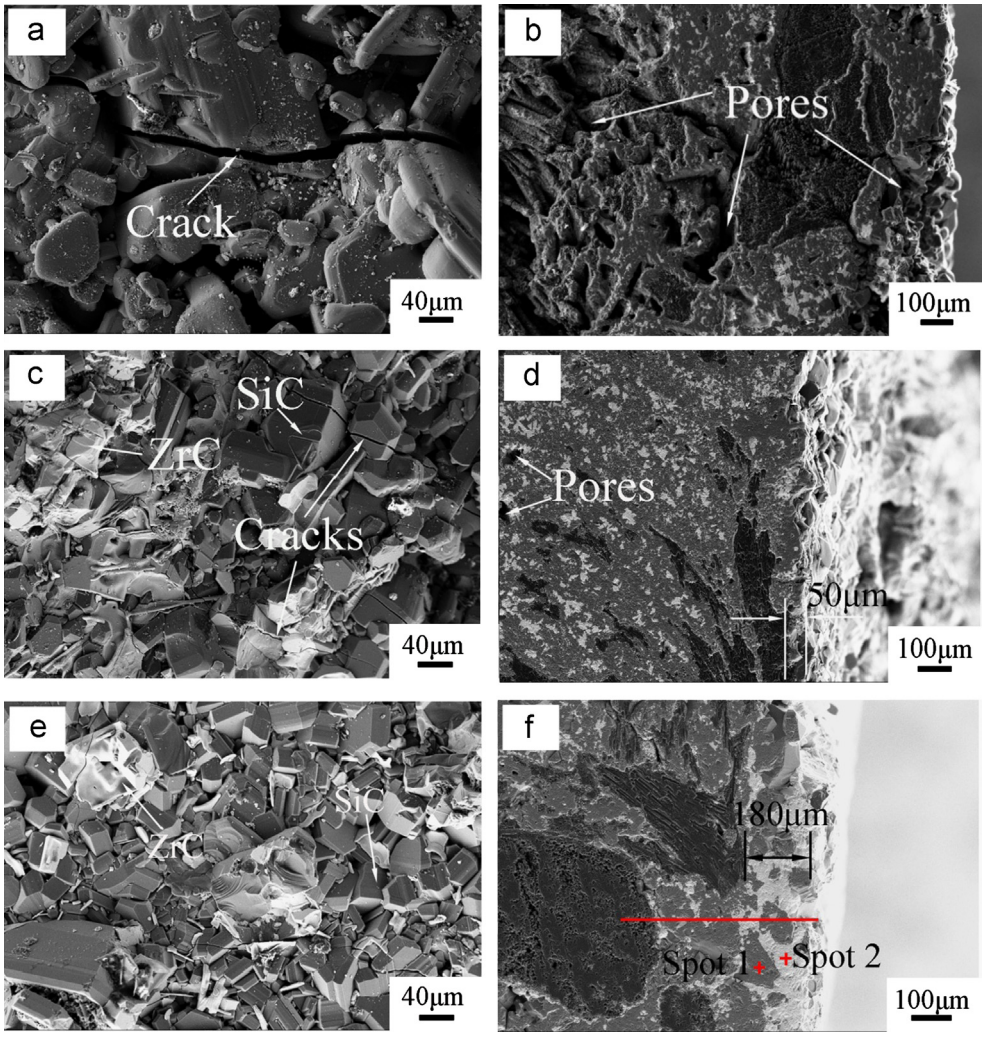

Fig. 2. Surface and cross-section SEM graphs of the 2D C/C−SiC−ZrC composites: (a, b) CSZ-1; (c, d) CSZ-2 and (e, f) CSZ-3. (For interpretation of the references to color in this figure legend, the reader is referred to the web version of this article.)

3. Results and discussion

3.1. Microstructure of the composites

It is well known that ICVI is the best process for the fabrication of C/C composites owing to its excellent controllability, uniform microstructure and good properties of the composites fabricated, and its significance for the mass manufacture of special-shape parts. So we use the ICVI process to prepare the porous C/C skeletons for 2D C/C–SiC–ZrC composites. Fig. 1 shows the microstructures of the C/C skeletons with different densities. It can be found that the thickness of pyrocarbon (PyC) increases along with the increase of the ICVI time and the as-prepared composites have homogeneous microstructure and uniform porosity distribution. There are three basic pore types in C/C skeletons: inter-fibre pores existing among fibres in a bundle; inter-bundle pores existing among fibre bundles in a fabric layer; and inter-layer pores existing among two layers of fabric [20]. The smaller inter-fibre pores can be easily filled by PyC in the ICVI

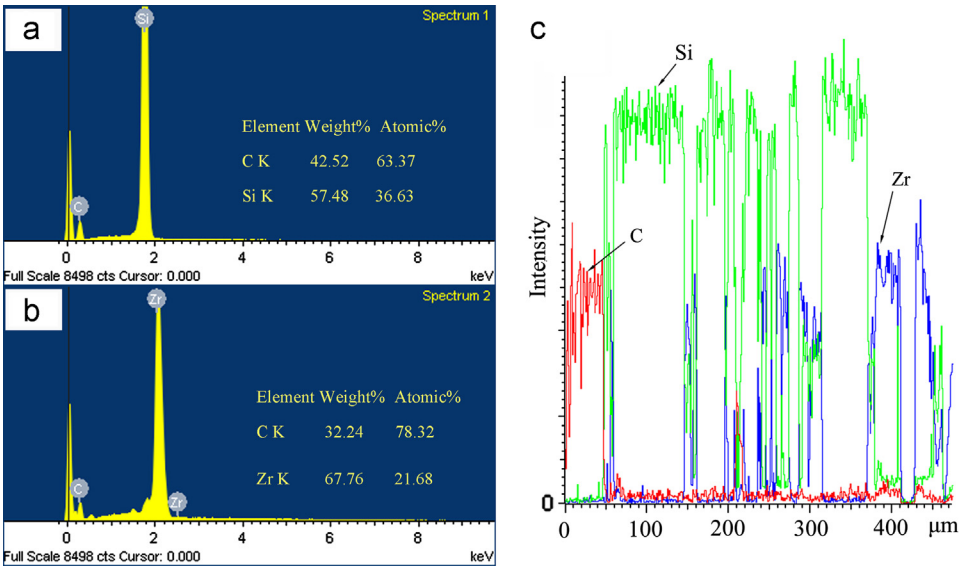

Fig. 4. The linear and point EDX analyses at the cross-section of composites CSZ-3: (a) EDX analysis of spot 1; (b) EDX analysis of spot 2 and (c) elements linear distributions (red line in Fig. 2(f)).

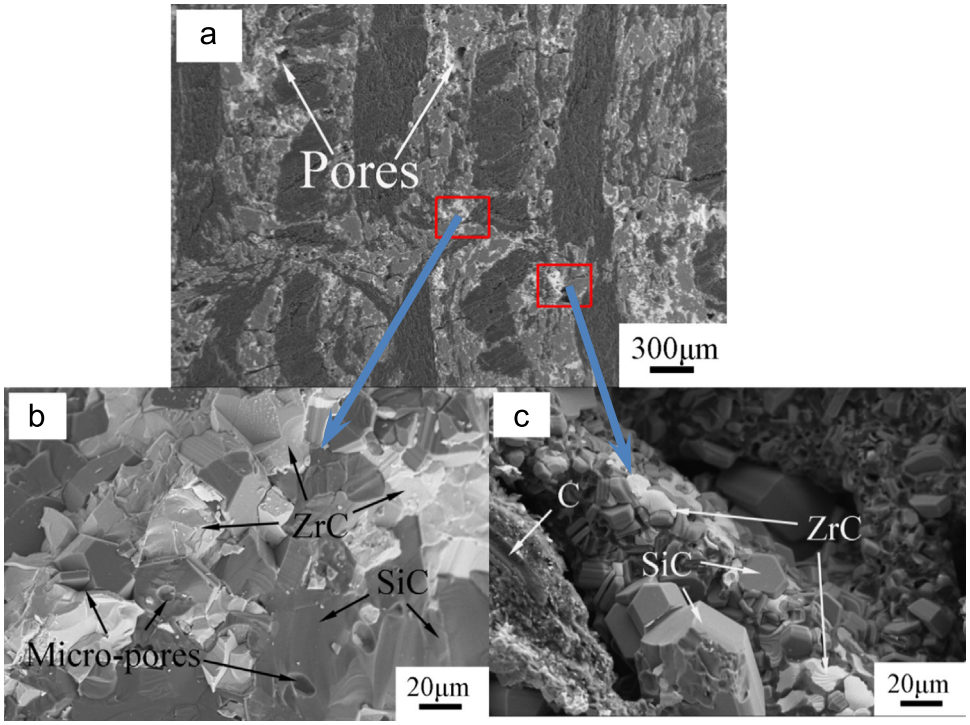

Fig. 5. (a) The inner microstructure of composites CSZ-3; (b) the large magnification of SiC–ZrC matrix and (c) the large magnification of pores.

process, but the larger inter-bundle and inter-layer pores are difficult to be completely densified in short time, which are considered as the infiltration channels for the molten powders during the following RMI process.

Table 1 presents the density and open porosity of the C/C composites and the C/C−SiC−ZrC composites; it can be seen that the composites prepared by the ICVI process have a high open porosity, the density of CSZ-1, CSZ-2 and CSZ-3 has increased by 58.93%, 50.00% and 23.18% compared with the porous skeletons CC-1, CC-2, and CC-3, respectively, and the open porosity have a great reduction. The pores in the skeletons have been filled up during the RMI process. Moreover, the closed porosity of the C/C skeletons prepared by the ICVI process is rather low, and the closed pores are hard to be filled up in the following RMI process.

Fig. 2 shows the surface and cross-section SEM graphs of the 2D C/C−SiC−ZrC composites. There is a rough coating consisting of two kinds of crystalline particles (grey and white phases) on the surface of composites, and the microstructure of the C/C−SiC−ZrC composites is clearly affected by the density of the C/C skeletons. According to the XRD and EDX analysis results (Fig. 3and 4(a) and (b), respectively), the coating on the surface is mainly composed of SiC (grey phase) and ZrC (white phase). It can be seen that the composite CSZ-1 has a rough and loose surface consisting of coarse crystalline particles and some bigger cracks existing in the coating. The cracks are caused by the different thermal expansion stresses between the coating and matrix in the cooling process after high-temperature infiltration. There are also many pores that survived after the RMI process, which presents that the pores could not be completely filled when the density of the C/C skeleton was low. The surface and cross-section SEM graphs of CSZ-2 shows that the coating and matrix are dense and well combined with each other. The thickness of the coating is approximately 50 μm. Furthermore, the SiC–ZrC coating on CSZ-3 is very dense without obvious penetrable cracks, and the thickness of the coating is approximately 180 μm. Fig. 4(c) shows the cross-section linear EDX analysis at a cross-section of composites CSZ-3. It can be seen that the phases of ZrC and SiC (shown as white and grey phase, respectively) disperse equably in the coating. The distribution of Si, representing SiC, in the binding site and the interior of the matrix leads to the good combination between the coating and matrix. The SiC–ZrC coating acts as an oxygen diffusion barrier for C/C composites and reacts with oxygen to form zirconium dioxide and silicon dioxide in oxyacetylene flame. The interactive combination state presented by coating and matrix on CSZ-2 and CSZ-3 indicates that a strong bonding force exists between them, which conducive to the improvement of the thermal shock resistance of the coatings. Hence, the as-prepared C/C–SiC–ZrC composites have better microstructure when the density of porous C/C skeletons is higher.

Fig. 5 shows an inner cross-section of CSZ-3. It can be seen that the SiC–ZrC matrix is formed deeply between the bundles and the layers. As seen from Fig. 5(b), the generated matrix is dense except for a few microscopic voids in it. The distribution of SiC–ZrC is not even, which is caused by the pore distribution in porous C/C skeleton. Moreover, the large inter-bundle and inter-layer pores are not completely filled (Fig. 5(c)), so there is a density gradient from the centre to the surface of sample. In addition, the surface of the pores has been covered by a dense SiC–ZrC layer, which could also prevent the C/C matrix from being exposed to oxidizing atmosphere.

According to the above analysis, the mechanism for the formation of the C/C−SiC−ZrC can be concluded as follows: during the RMI process, the molten Si and Zr ware infiltrated into the porous C/C skeletons by capillary forces along the carbon fibre bundles, and reacted with the deposited PyC to form C–SiC–ZrC matrix at a high temperature. SiC–ZrC coating, meanwhile, formed on the surface of the matrix by chemical combination with good bonding strength. The following reactions would happen during the RMI process [17,19,21]:

$$Si(l) + Zr(l) \rightarrow ZrSi_2(l) \quad (1)$$

$$Si(l) + C(s) \rightarrow SiC(s) \quad (2)$$

$$Zr(l) + C(s) \rightarrow ZrC(s) \quad (3)$$

$$ZrSi_2(l) + C(s) \rightarrow SiC(s) + ZrC(s) \quad (4)$$

3.2. Mechanical properties of the composites

The mechanical test results are summarized in Table 2. It is clear that the bending properties of the C/C composites increase

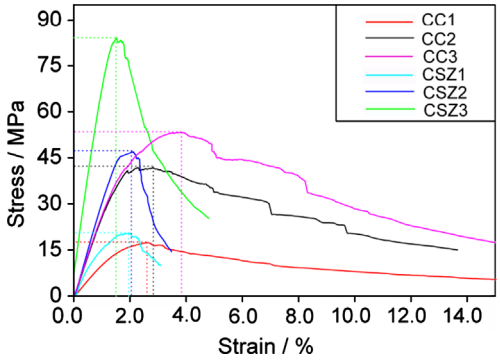

Fig. 6. Stress−strain curves of the C/C composites and the C/C−SiC−ZrC composites.

Table 2
Bending properties of the C/C composites and the C/C–SiC–ZrC composites.

Samples	CC-1	CC-2	CC-3	CSZ-1	CSZ-2	CSZ-3
Bending strength (MPa)	17.40 ± 2.23	41.78 ± 1.14	53.35 ± 3.08	20.14 ± 1.08	47.02 ± 4.06	70.57 ± 6.11
Bending modulus (GPa)	0.09 ± 0.01	0.24 ± 0.03	0.31 ± 0.13	4.66 ± 1.10	6.11 ± 1.06	13.19 ± 2.15

with density and those of the C/C–SiC–ZrC composites improve after the RMI process. The bending modulus and bending strength of CSZ-3 reach 13.19 GPa and 70.57 MPa, respectively. It is notable that the infiltration temperature is 2300 °C and there may be some damage to the fibre preform during the preparation. In order to fabricate C/C–SiC–ZrC composites with good mechanical properties, the pre-prepared C/C skeletons should have an appropriate density (about 1.51 g/cm^3).

Fig. 6 shows the stress−strain curves of the two kinds of composites. They indicate that all the composites present pseudo-plastic behaviour, which is attributed to the crack deflection, interfacial debonding and fibre pull-out (Fig. 7). However, the fracture strains of C/C–SiC–ZrC composites are smaller than those of C/C composites. It is well known that good mechanical properties of the composites largely depend on the fibre−matrix and the fibre−matrix−filler interfacial adhesion, since the load transfer from the matrix to the fibres would require a good bonding at the interfaces [20]. But there are large amounts of pores in the porous C/C composites, so the fibres cannot be solidly bonded by the deposited PyC, especially between the fibre bundles and layers. Lower open porosity is advantageous for the load transfer to the fibres, which results in that the bending properties increasing with density (Table 1, Fig. 7(a)−(c)). As for the C/C–SiC–ZrC composites, they have a structure of carbon fibres covered by the deposited PyC and SiC–ZrC matrix (Fig. 5(b)), and the

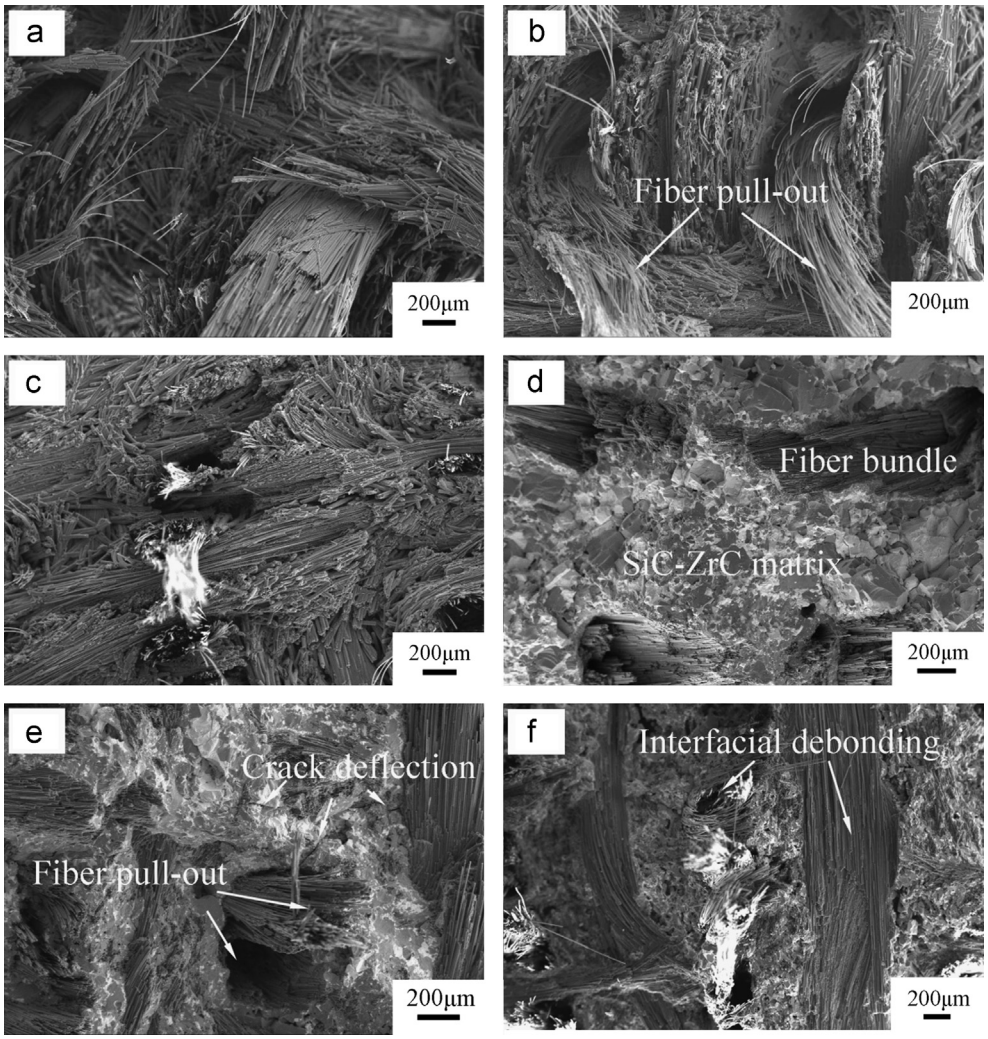

Fig. 7. Fracture surfaces of the C/C composites and the C/C−SiC−ZrC composites: (a) CC-1; (b) CC-2; (c) CC-3; (d) CSZ-1; (e) CSZ-2 and (f) CSZ-3.

Table 3
Ablation properties of the C/C composites and the C/C–SiC–ZrC composites.

Samples	CC-1	CC-2	CC-3	CSZ-1	CSZ-2	CSZ-3		
Ablation time (s)	30	30	30	30	30	30	60	90
Linear ablation rate ($\times 10^{-3}$ mm/s)	3.25 ± 0.12	3.75 ± 0.07	3.75 ± 0.11	2.33 ± 0.12	1.33 ± 0.05	0.67 ± 0.04	0.33 ± 0.03	1.44 ± 0.07
Mass ablation rate ($\times 10^{-3}$ g/s)	1.59 ± 0.06	1.24 ± 0.13	0.94 ± 0.05	2.06 ± 0.15	1.65 ± 0.06	0.24 ± 0.02	0.28 ± 0.06	0.21 ± 0.03

SiC–ZrC matrix does not simply physically adhere but truly chemically bonded to the fibre surfaces due to the participation of PyC from the fibre surface in the active carbothermal reaction (Reactions (2)–(4)) [22]. Under bending load, the cracks propagation is difficult along the layers due to the smaller amount of large pores and the stronger matrix between the layers after the RMI process. When cracks develop between the bundles or between the layers, the SiC–ZrC matrix acts as an effective crack deflector to prevent direct crack propagation and thus produces many secondary cracks (Fig. 7(e, f)).

3.3. Ablation behaviour of the composites

Table 3 shows the ablation test results of the C/C composites and the C/C–SiC–ZrC composites; it can be seen that the C/C–SiC–ZrC composites show a lower average linear ablation rate compared with the C/C composites. However, the mass ablation rates of the C/C–SiC–ZrC composites present two different kinds of situations: the mass erosion of CSZ-1 and CSZ-2 increases after the RMI process, but CSZ-3 has steady ablation resistance for 90 s.

For the 2D ICVI C/C composites, the exterior inter-bundle pores are very easily attacked during the ablation process, resulting in the possible formation of macroscopic ablation pits and a heterogeneous ablation front. The ablation morphology and EDX analysis of the 2D C/C−SiC−ZrC composites

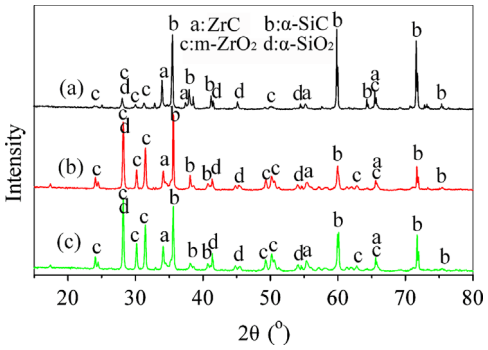

Fig. 9. XRD patterns of the surface of composites CSZ-3 after ablation for different times: (a) 30 s; (b) 60 s and (c) 90 s.

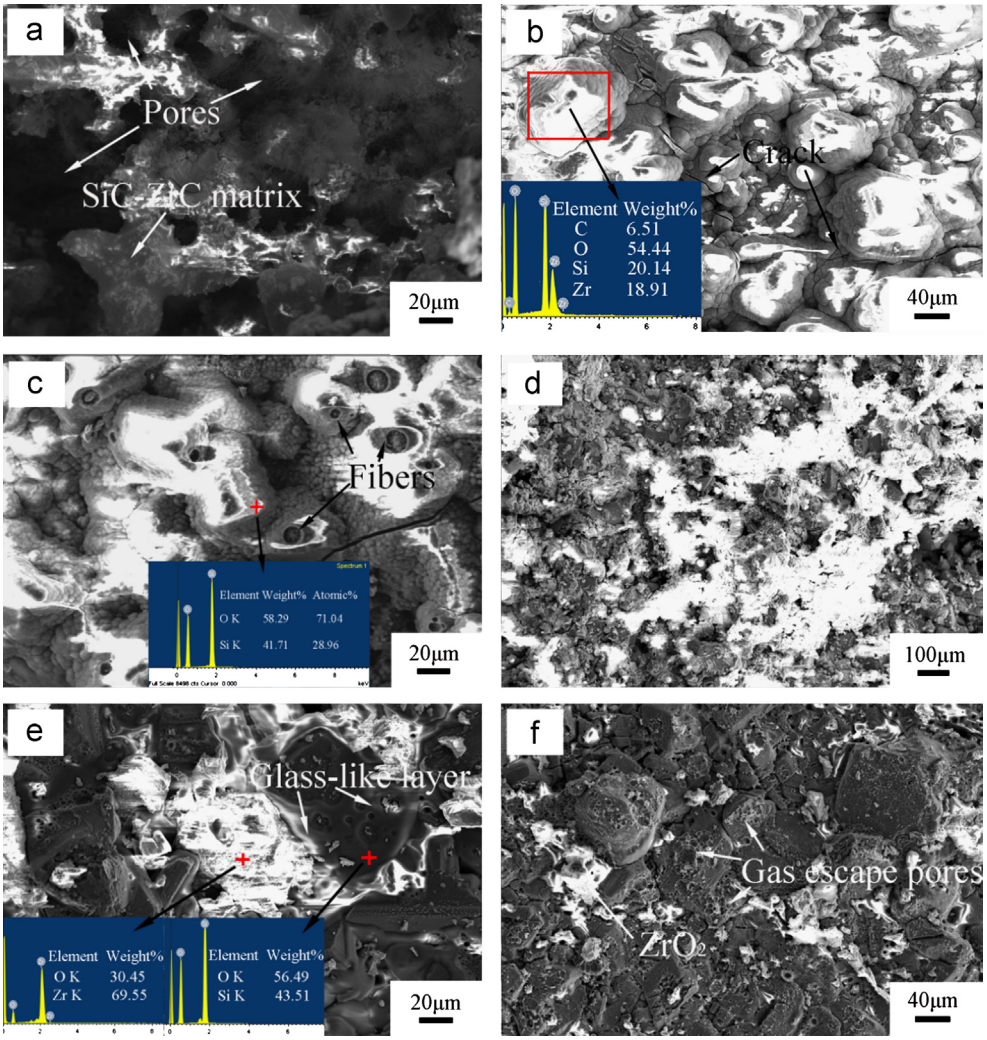

Fig. 8. Ablation morphology and EDX analysis of the C/C−SiC−ZrC composites ablated for 30 s: centre region and outer region of CSZ-1 (a, b); centre region and outer region of CSZ-2 (c, d) and centre region and outer region of CSZ-3 (e, f).

ablated for 30 s are shown in Fig. 8. An obvious macroscopic pit can be found at the ablation centre of CSZ-1 because its loose matrix structure cannot endure the high-pressure and ultrahigh temperature under oxyacetylene torch (Figs. 2(b) and 8(a)). A dense white layer also can be seen in the outer region of the ablated surface (Fig. 8(b)). EDX and XRD patterns (Figs. 8(b) and 9, respectively) of the ablated samples indicate that the white layer is mixed oxides consisting of SiO_2 and ZrO_2 which are generated by the thermochemical reaction during the ablation process [21]. As shown in Fig. 8(c) and (d), the erosion for CSZ-2 is better than that for CSZ-1. There is no obvious pit in the centre region and the fibres are surrounded with dense mixture SiO_2 layers. Fig. 8(e) and (f) shows the erosion surface of CSZ-3. Only slight ablation occurred on the surface of the samples and dense SiC–ZrC coating can resist the ablation by forming a protective glass-like oxide layer. Through the point EDX analysis in Fig. 8(e), it is known that the main component of the glass-like oxide layer is SiO_2 and the white phase is ZrO_2. The melting points of ZrO_2 and SiO_2 are 2700 °C and 1723 °C, respectively, while the temperature of the ablation centre is about 2300 °C, so SiO_2 exists as liquid phase in the centre region during the ablation process [21], while solid-state ZrO_2 could help to prevent the loss of liquid phase SiO_2 under high temperature air scour. In the outer region, less coating has been oxidized and no glass-like oxide layer can be found on the surface of the composites due to the lower ablation temperature (Fig. 8(f)).

In order to further study the ablation resistance of CSZ-3, ablation tests with longer time have been carried out. Figs. 10 and 11 present the ablation morphology of CSZ-3 ablated for 60 s and 90 s, respectively. Fig. 10 indicates that the SiC–ZrC coating on the surface of CSZ-3 still efficiently protects the composites from ablation. It can be seen that with the extension of ablation time, the glass-like oxide layer has been scoured off by flux and many erosion pits formed on the SiC grains (Fig. 10(a)). But survival ZrO_2 existing in the centre region could enhance the anti-erosion property of the coating by improving the mechanical erosion resistance. It is interesting that the temperature in the outer region increased when the samples were ablated for 60 s, resulting in the formation of

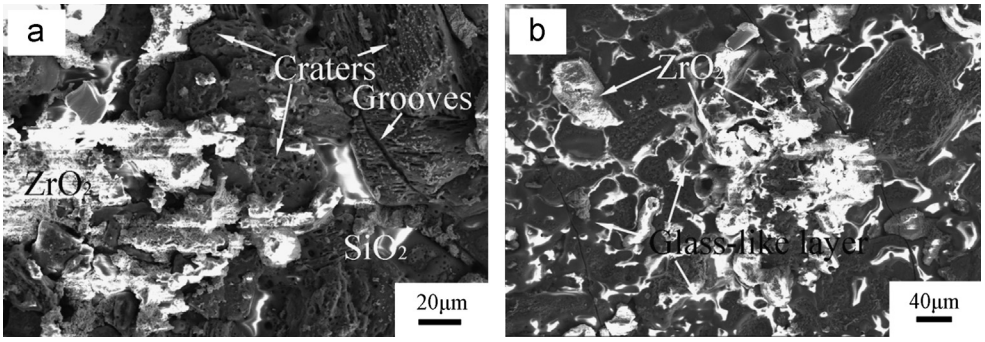

Fig. 10. Ablation morphology of CSZ-3 ablated for 60 s: (a) centre region and (b) outer region.

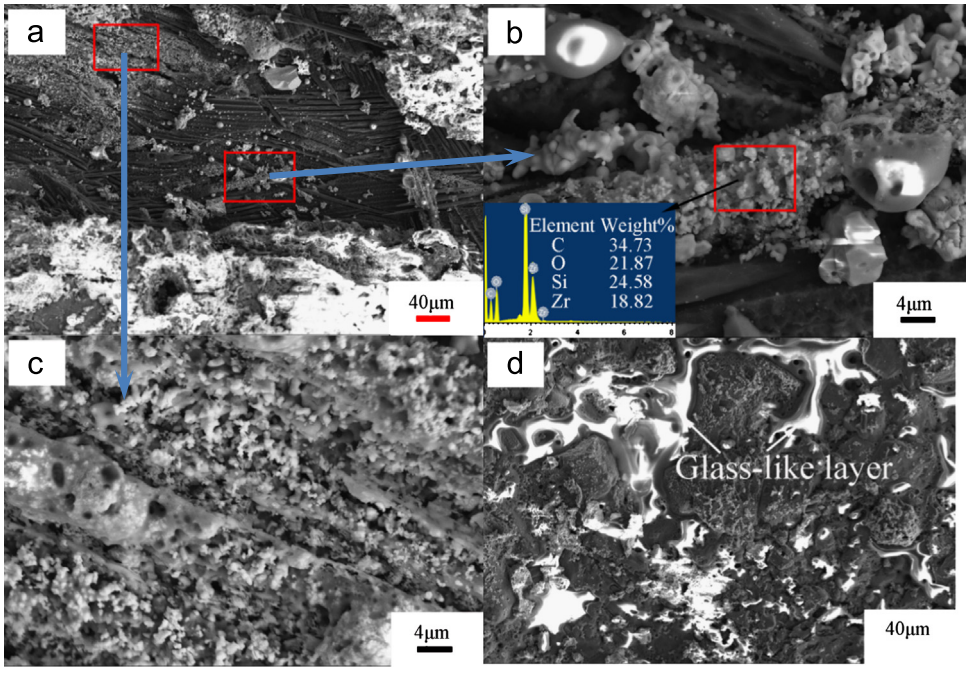

Fig. 11. Ablation morphology and EDX analysis of CSZ-3 ablated for 90 s: (a) centre region; (b, c) large magnification of (a) and (d) outer region.

glass-like layer mixed by SiO_2 and ZrO_2 in this region (Fig. 10(b)). Fig. 11 indicates that in ablation centre region, SiC–ZrC coating on the CSZ-3 surface is ablated thoroughly after ablation for 90 s, but the SiC−ZrC matrix provides further ablation resistance for the composites. The fibres are covered with some white phase in Fig. 11(b) and (c), which could help to protect the fibres from further ablation. In addition, the dense PyC also has a lower ablation rate. Although the linear ablation rate of CSZ-3 increased after ablation for 90 s, the matrix was still well protected without serious erosion. The ablation of SiC−ZrC coating in outer region is tiny (Fig. 11(d)).

As has been analysed above, the density of the C/C skeletons is an important factor affecting the mechanical properties and ablation behaviour of the C/C–SiC–ZrC composites prepared by the RMI process. When the density of the C/C skeletons is 1.12 g/cm^3, the structure of CSZ-1 is loose, generating poor bending properties and higher ablation rates. When the density of the C/C skeletons is 1.51 g/cm^3, dense SiC−ZrC matrix forms inside the skeleton by chemical reaction and dense SiC−ZrC coating forms on the surface of CSZ-3. The main ablation mechanism of the C/C−SiC−ZrC composites is a combined effect of thermochemical and mechanical erosion. The dense coating on the surface of CSZ-3 reacted with the oxygen in oxyacetylene flame; then an oxide layer consisting of SiO_2 and ZrO_2 formed on the coating, which could prevent the oxygen from contacting with the SiC−ZrC coating. Moreover, the SiC−ZrC matrix and layer on the fibres provide further ablation resistance when the surface coating burned through after long time ablation. In addition, the gas escape of CO and SiO generated by the thermochemical reactions and the evaporation of SiO_2 will result in a thermal barrier effect, which can effectively hold back the heat transfer into the composites [20].

4. Concluding remarks

2D C/C–SiC–ZrC composites were prepared by ICVI combined with the RMI method using various density porous C/C skeletons. The mechanical properties and ablation behaviour of C/C–SiC–ZrC composites are remarkably influenced by the density of porous C/C skeletons. The composites CSZ-3 fabricated using C/C skeletons with a density of 1.51 g/cm^3 have dense structures and a SiC−ZrC coating forms on the surface. The bending modulus and strength of CSZ-3 are 13.19 GPa and 70.57 MPa, respectively. The linear and mass ablation rates of CSZ-3 ablated for 90 s are 1.44×10^{-3} mm/s and 0.21×10^{-3} g/s, respectively. The main ablation mechanism of the C/C−SiC−ZrC composites is a combined effect of thermochemical and mechanical erosion. The dense SiC−ZrC coating and its oxide layer play an important role during ablation, and the gas escape and evaporation will result in a thermal barrier effect, which can effectively hold back the heat transfer into the composites.

Acknowledgements

This work has been supported by the National Natural Science Foundation of China under Grant no. 50832004, the "111" Project of China under Grant no. B08040, and the Research Fund of State Key Laboratory of Solidification Processing (NWPU), China (Grant nos. G8QT0222 and 25-TZ-2009).

References

[1] R. Savino, Aerothermodynamic study of UHTC-based thermal protection systems, Aerospace Science and Technology 9 (2005) 151–160.
[2] A. Tsukahara, H. Yamao, Advanced thermal Protection Systems for Reusable Launch Vehicles, 2001 AIAA-2001-1909.
[3] Y. Yang, Research progress on thermal protection materials and structures of hypersonic vehicles, Applied Mathematics and Mechanics 29 (2008) 51–60.
[4] H.J. Li, Carbon/carbon composites, New Carbon Materials 16 (2001) 79–80.
[5] E. Fitzer, The future of carbon–carbon composites, Carbon 25 (1987) 163–190.
[6] J.C. Han, X.D. He, S.Y. Du, Oxidation and ablation of 3D carbon −carbon composite at up to 3000 °C, Carbon 33 (1995) 473–478.
[7] J.E. Sheehan, Oxidation protection for carbon fibre composites, Carbon 27 (1989) 709–715.
[8] T.L. Dhami, O.P. Bahl, B.R. Awasthy, Oxidation-resistant carbon −carbon composites up to 1700 °C, Carbon 33 (1995) 479–490.
[9] D.D. Jayaseelan, R.G. Sá, P. Brown, W.E. Lee, Reactive infiltration processing (RIP) of ultra high temperature ceramics (UHTC) into porous C/C composite tubes, Journal of the European Ceramic Society 31 (2011) 361–368.
[10] Z.F. Chen, D. Fang, Y.L. Miao, B. Yan, Comparison of morphology and microstructure of ablation canter of C/SiC composites by oxy-acetylene torch at 2900 and 3550 °C, Corrosion Science 50 (2008) 3378–3381.
[11] X.T. Shen, K.Z. Li, H.J. Li, Q.G. Fu, S.P. Li, F. Deng, The effect of zirconium carbide on ablation of carbon/carbon composites under an oxyacetylene flame, Corrosion Science 53 (2011) 105–112.
[12] Q.F. Tong, J.L. Shi, Y.Z. Song, Q.G. Guo, L. Liu, Resistance to ablation of pitch-derived ZrC/C composites, Carbon 42 (2004) 2495–2500.
[13] Q.G. Fu, H.J. Li, X.H. Shi, K.Z. Li, G.D. Sun, Silicon carbide coatings to protect carbon/carbon composites against oxidation, Scripta Materialia 52 (2005) 923–927.
[14] O. Yamamoto, T. Sasamoto, M. Inagaki, Anti-oxidation of carbon −carbon composites by SiC concentration gradient and zircon over-coating, Carbon 33 (1995) 359–365.
[15] W. Qiang, Zirconium, Mechanical Industry Publishing Company, China, 1961.
[16] E.K. Storms, The Refractory Carbides, Academic Press, New York, 1967.
[17] Y.G. Wang, X.J. Zhu, L.T. Zhang, L.F. Cheng, C/C–SiC–ZrC composites fabricated by reactive melt infiltration with $Si_{0.87}Zr_{0.13}$ alloy, Ceramics International 38 (2012) 4337–4343.
[18] H.T. Wu, X. Wei, S.Q. Yu, W.G. Zhang, Ablation performances of multi-phased C/C−ZrC−SiC ultrahigh temperature composites, Journal of Inorganic Materials 26 (2012) 852–856.
[19] Z.Q. Li, H.J. Li, S.Y. Zhang, K.Z. Li, Microstructure and ablation behaviours of integer felt reinforced C/C–SiC–ZrC composites prepared by a two-step method, Ceramics International 38 (2012) 3419–3425.
[20] S.F. Tang, J.Y. Deng, W.C. Liu, K. Yang, Mechanical and ablation properties of 2D carbon/carbon composites pre-infiltrated with a SiC filler, Carbon 40 (2006) 2877–2882.
[21] Z.Q. Li, H.J. Li, S.Y. Zhang, J. Wang, W. Li, F.J. Sun, Effect of reaction melt infiltration temperature on the ablation properties of 2D C/C–SiC–ZrC composites, Corrosion Science 58 (2012) 12–19.
[22] H. Zou, N. Wali, J.M. Yang, N.P. Bansal, Microstructural development of a C_f/ZrC composite manufactured by reactive melt infiltration, Journal of the European Ceramic Society 30 (2010) 1527–1535.